Multichannel Photoinduced Intramolecular Electron-Transfer Excitations in a Bis-naphthalimide Spermine Conjugate by Time-Dependent Density Functional Theory

Juan-Qin Li and Xiang-Yuan Li*

College of Chemical Engineering and State Key Laboratory of Biotherapy, Sichuan University, Chengdu 610065, P. R. China

Received: June 22, 2007

Density functional theory was applied to the investigation of photoinduced electron transfer (ET) and the absorption spectrum for a bis-naphthalimide spermine conjugate. The multichannel feature of ET excitation in this system was focused on because four groups may act as electron donors and acceptors. The segment in this conjugate, *N*-(*N*-methylpropyl)-1,8-naphthalimide, which contains one donor and acceptor pair, was studied at first. Through theoretical calculation, the absorption band at 340 nm was assigned to the $\pi \rightarrow \pi^*$ transition. For the whole system involving four chromophores, this work suggested three types of ET. From the theoretical investigation, the naphthalimide radical anion turned out to be formed via intramolecular ET between the two terminal naphthalimide groups, rather than via the electron transfer between the dialkylamine moiety and the naphthalimide one. Furthermore, the electronic coupling matrix elements according to the generalized Mulliken−Hush theory were estimated and the detailed analyses showed that the strongest absorption was due to the local excitation of the naphthalimide chromophore.

Introduction

Photoinduced ET is a fundamental process in many biological and biochemical reactions, and its applications have received much attention. Researches in this field have extended to the design of the molecular device.[1−5] The systems involving naphthalimide and polyamine chromophores have attracted much attention in the past decades because of their anticancer activity.[6−10] Naphthalimide was used as photosensitizes and is well-known to be harmful because it can cause DNA damage by the one-electron oxidation mechanism.[11−14]As described by Kawai and co-workers, photosensitized DNA damage by naphthalimide can be induced by oxidation through electron transfer from DNA to the singlet or triplet of naphthalimide.[15] In 1995, Saito et al. demonstrated the photoinduced DNA cleavage via ET between a guanine base and 1,8-naphthalimide.[11] Furthermore, it was illustrated that the versatility of naphthalimide derivatives is initiated by N-substituted 1,8-naphthalimide chromophores.[16] The substituted naphthalimide chromophores, which were used as fluorescent probes in biological cells[17] and laser dyes,[18] were described in detail by Middleton et al.,[19,20] and 1,8-naphthalimide was widely used in chemosensors and fluorescent labels in the past.[21−24] In the recent years, 1, 8-naphthalimide was also used as optical switches by changing their chemical surroundings,[25] e.g., the nature of the solvent and the presence of certain cations.[26] Such systems have been foreseen to open new perspectives for the realization of artificial functions at the molecular level. Aveline et al. characterized the photochemistry of various N-substituted 1,8-naphthalimide and 1,4,5,8-naphthaldiimides.[27] The polyamines of spermidine and spermine are growth factors in both eucaryotic and procaryotic cells and exist as polycations at physiological pH. If synthesis of polyamines is blocked, cell growth will stop or terribly slow down. Although their exact functions have not yet been identified, it is clear that polyamines play important roles in cellular processes such as replication, transcription, and translation. In the early 1990s, the bis-naphthalimido compounds, which contain two naphthalimido rings and covalently attach at the end of a linker chain containing nitrogen atoms, were synthesized and their anticancer properties were evaluated.[28] The compounds with a chain containing nitrogen atoms were previously synthesized by simply reacting the corresponding alkyltetraamine with 1,8-naphthalic anhydrides.[29] The increase of nitrogen atoms in the linker chain significantly improves their aqueous dissolution properties and reduces the cytotoxic activity.[30] It is obvious that both the bis-naphthalimide group and the polyamine chain appear to be important for the biological activity.

As shown in Scheme 1, the model molecule, bis-naphthalimide spermine (BNS) conjugate, consists of two *N*-(*N*-methylpropyl)-1,8-naphthalimide (MNP) fragments. The four groups, two terminal conjugated groups and two intermediated −NH− groups, can be expected to act as the electron donors and acceptors. Therefore, there are possibly different types of charge-transfer (CT) states. Recently, Jones and co-workers introduced hypotheses of ET in BNS system,[31] but which of the competitive ET processes is more possible still remains unclear. In addition, it is still blurry that the maximum absorption band at 340 nm of BNS in acetonitrile results from local excitation (LE) or CT excitation. In the present work, we tried to make clear the above problems through theoretical investigation. A significant feature presented in this work for the model system is that there are various types of the photoinduced intramolecular ETs, due to the existence of the four donor and acceptor sites involved in this model molecule. So, this molecule can serve as an ideal model system for the multichannel ETs via photoexcitation. For the sake of convenience, the four donor and acceptor groups in BNS are denoted, from left to right, as NP1, SP1, SP2, and NP2. The excitation of BNS will result in the intramolecular ET, but the electron donor or the acceptor is

* Corresponding author. Tel.: +862885405233. Fax: +862885407797. E-mail: xyli@scu.edu.cn.

10.1021/jp074883t CCC: $37.00
Published on Web 11/22/2007

SCHEME 1

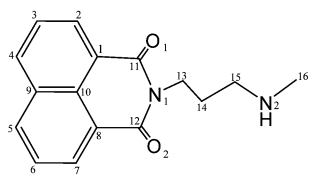

MNP

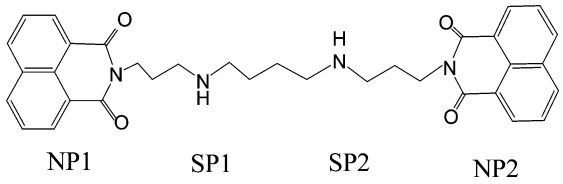

NP1 SP1 SP2 NP2

BNS

not unique. The possible ET processes are, from SP1 to NP1, from SP1 to NP2, from SP2 to NP1, from SP2 to NP2, from NP1 to NP2, and conversely from NP2 to NP1.

This work was organized as follows. The methodology and computational details were briefly described in the next section. The results and discussions were presented in the following section, including the absorption/emission properties of MNP both in the gas phase and in acetonitrile, and the driving force for the photoinduced ET was also investigated. Comparative discussions with experimental observations were made. Furthermore, the structures of a number of photoexcited states of BNS and the solvent effect were reported. The electronic coupling matrix elements for the transition from the ground state to the specified states were estimated. The conclusions were given in the last section.

Methodology and Computational Details

Methodology. According to Fermi's golden role, the electron-transfer (ET) rate constant, k_{et}, is proportional to the square of the electronic coupling matrix element H_{ij}, i.e.,[32−34]

$$k_{et} = \frac{2\pi}{\hbar} H_{ij}^{\ 2}(\mathrm{FCWD}) \tag{1}$$

where $\hbar = h/2\pi$, with h being Planck's constant. The electronic coupling matrix element between the initial and final diabatic state Ψ_i and Ψ_j is defined as

$$H_{ij} = \langle \Psi_i | \mathbf{H} | \Psi_j \rangle \tag{2}$$

FCWD in eq 1 is a density-of-state weighted Franck−Condon factor taking into account the density of vibrational levels and the Franck−Condon overlap. This overlap incorporates the vibrational modes of the molecule, $\{\omega_i\}$, and those of the solvents, $\{\omega_s\}$.[35] If the condition of $h\omega_i \gg k_B T$ (here k_B denotes the Boltzmann constant) is satisfied, the vibrational modes of the molecule can be treated quantum mechanically, and a classical description can be taken for the solvent vibrational modes in such a case, the Franck−Condon factor can be written as[36]

$$\mathrm{FCWD} = \left(\frac{1}{4\pi\lambda_s k_B T}\right)^{1/2} \sum_v \mathrm{e}^{-S} \frac{S^v}{v!} \exp\left[-\frac{(\Delta G^0 + \lambda_s + v\hbar\langle\omega_i\rangle)^2}{4\lambda_s k_B T}\right] \tag{3}$$

where λ_s denotes the solvent reorganization energy, ΔG^0 is the variation of the Gibbs free energy in the reaction, and S is the Huang−Rhys factor, i.e.,

$$S = \frac{\lambda_i}{\hbar\langle\omega_i\rangle} \tag{4}$$

where $\hbar\langle\omega_i\rangle$ is the effective mode vibrational energy and λ_i is the inner reorganization that is responsible for the energy required to accommodate the nuclear rearrangements occurring upon ET when going from the equilibrium geometry of the initial state to that of the final state.

To estimate the ET rate constant, k_{et}, and to study further the character of absorption spectra, the generalized Mulliken−Hush (GMH) theory for the nonperturbative calculation of H_{ij} of ET was employed in this work. Cave and Newton[37] developed the GMH formalism and expressed H_{ij} as

$$H_{ij} = \frac{m_{ij}\Delta E_{ij}}{\sqrt{(\Delta\mu_{ij})^2 + 4(m_{ij})^2}} \tag{5}$$

where ΔE_{ij} is the energy gap between the initial adiabatic state and the final one, $\Delta\mu_{ij}$ is the dipole moment difference between states i and j, and m_{ij} denotes the transition dipole moment connecting the two states.

Computational Details. Prior to the calculation of excited states, the ground-state geometries were optimized using density functional theory (DFT), by employing B3LYP functional with 6-31G* basis sets for MNP and 6-31G basis sets for BNS. All the calculations were carried out using the Gaussion03 program. Vertical transitions were assumed first, and the calculated excitation energies could be identified by comparing with the band maxima in the experimental spectra. According to the calculations here, the excitation energies depend weakly on basis sets, and the addition of the polarized functionals only leads to small influence (about 0.10 eV) on the transition energies. In this work, the 6-31G basis sets were used to calculate the low-lying excited states of BNS. The optimized geometry is confirmed by a frequency analysis. The ground-state geometries were employed throughout all the calculations of the excited states, based on the Franck−Condon principle.

The time-dependent DFT (TD-DFT) has been proved suitable for the calculation of electronic excitations.[38−41] The functionals used to calculate the energies of excited states in this work are the same as those used in the geometry optimization. It is well-known that solvent has great influence on the electronic spectra owing to the solvent polarization. In this work, the solvent effect has been considered using the polarizable continuum model (PCM), and all the calculations are performed in acetonitrile. Recently, we made modifications on the nonequilibrium solvation theories in the framework of continuum model, and new formulations for the spectral shift were presented elsewhere.[42−44] However, for the absorption spectrum of the present model systems, the electronic excitation is due to the transition from a charge-balanced state to a charge-separated one. In such cases, no considerable error is expected when the traditional numerical algorithm coded into the quantum mechanical package is adopted. Therefore, the traditional continuum model that was linked to Gaussian 03 version is employed for the purpose of solvent effect estimation of the absorption spectrum.[45−48]

It is known that a single TD-DFT calculation cannot give the dipole moment of the excited state. In this work, the dipole

TABLE 1: Transition Energies, Oscillator Strengths, and Dipole Moments of MNP in the Gas Phase and in Acetonitrile[a]

	gas phase				acetonitrile					
state	dominant transition	E^b	f^c	μ^d	dominant transition	E^b	f^c	μ^d	$\Delta F^{non\ e}$	$E_{exp}{}^f$
T_1	HOMO → UMO	2.55	/	4.31	HOMO → LUMO	2.53	/	6.08		
		2.55		4.53		2.53		7.08		
T_2	HOMO−1 → LUMO	2.63	/	32.15	HOMO−1 → LUMO	2.80	/	29.99		
		2.91		32.09		3.06		19.90		
S_1	HOMO → LUMO	2.65	0.0001	31.27	HOMO → LUMO	2.78	0.0001	29.07	−0.38	
		2.91	0.0001	31.23		3.02	0.0001	29.03	−0.42	
S_2	HOMO−2 → LUMO	3.50	0.0002	5.85	HOMO−1 → LUMO	3.62	0.2670	8.55	−0.39	3.51
		3.66	0.0004	5.31		3.71	0.2813	8.49	−0.50	
S_3	HOMO−1 → LUMO	3.72	0.2059	5.92	HOMO−3 → LUMO	3.77	0.0003	3.54	−0.45	
		3.81	0.2173	5.87		3.92	0.0002	3.06	−0.42	
S_4	HOMO−3 → LUMO[g]	3.92	0.0002	3.78	HOMO−2 → LUMO	3.93	0.0329	7.62	−0.50	
		4.06	0.0027	1.25		4.03	0.0386	7.83	−0.56	
S_5	HOMO−3 → LUMO[g]	4.01	0.0096	1.13	HOMO−5 → LUMO	4.18	0.0097	2.47	−0.34	
	HOMO−5 → LUMO[h]	4.14	0.0123	0.77		4.32	0.0091	2.10	−0.36	

[a] Results using 6-31G* basis sets. For each transition, the first row is the results using B3LYP functional; the second row is the results by MPW1PW91 functional. [b] Relative energies with respect to the ground state, in eV. In the gas phase, the energies at the ground state are −879.33767 and −879.14024 au with B3LYP and MPW1PW91 functionals, respectively. The dipole moments are 4.08 and 3.86 D, respectively. In acetonotrile, the energies at the ground state are −879.35634 and −879.15453 au with B3LYP and MPW1PW91 functionals, respectively. The dipole moments are 6.08 and 6.11 D, respectively. [c] Oscillator strengths. [d] Dipole moments in Debye. [e] ΔF^{non} is the nonequilibrium solvation energy (electrostatic contribution in eV), which measures the electrostatic free energy difference between the nonequilibrium solvation state and the gas-phase case for the specified excited state. In Gaussian 03, a default option for the excited-state calculation corresponds to the nonequilibrium solvation state. The equilibrium solvation energy of the ground state is calculated to be −0.51 eV with B3LYP functional and −0.53 eV with MPW1PW91 functional. [f] Experimental values from refs 25 and 31. [g] Both S_4 and S_5 are mainly due to the transition from HOMO−3 to LUMO when the TD-B3LYP functional is used, but the expansion coefficients of configurations were found different. [h] MPW1PW91 functional.

moments for excited states were computed using the one-particle density matrix.[49] This method typically results in an overestimation of the dipole moment. Still, the calculated dipole moments will be useful when one state is compared to another.

Results and Discussion

Absorption and Emission Properties of MNP. To see insight into the intramolecular ET in the BNS conjugate, we calculated the electronic structure of the excited state of the separated species at first; thus the excitation mechanism of the whole molecule can be anatomized. The geometry of MNP was optimized at the B3LYP/6-31G* and MPW1PW91/6-31G* levels in vacuum, respectively. There is a slight difference in the structures of MNP optimized with B3LYP and MPW1PW91 functionals. The dipole moment of MNP at ground state is 4.08D by B3LYP and 3.86D by MPW1PW91 functional. In the following calculations, the excited states were investigated using their optimal ground-state structures with the two different functionals.

The vertical excitation energies, together with the dipole moments and the oscillator strengths of MNP (see Scheme 1) in the gas phase and in acetonitrile were calculated at B3LYP/6-31G* and MPW1PW91/6-31G* levels (Table 1), respectively. The frontier orbitals involved in the low-lying states of MNP were illustrated in Figure 1. For the MNP system, the first five lowest singlet excited states and first two triplet excited states were calculated.

The transition characters of MNP in acetonitrile are similar to those in the gas phase. As shown in Table 1, our results indicate that two kinds of functionals give almost the same energy order and the same transition feature for the low-lying excited states of MNP. We focus on the cases in acetonitrile as the experiment was carried out in solution. The calculated results indicate that the T_2 and S_1 are CT states and others are LE states. Experimental study indicated that the ground-state aggregation process facilitates the formation of radical anion. The value of the free energy of ground-state dimerization has been experimentally determined to be −0.13 eV for a pyrene chromophore

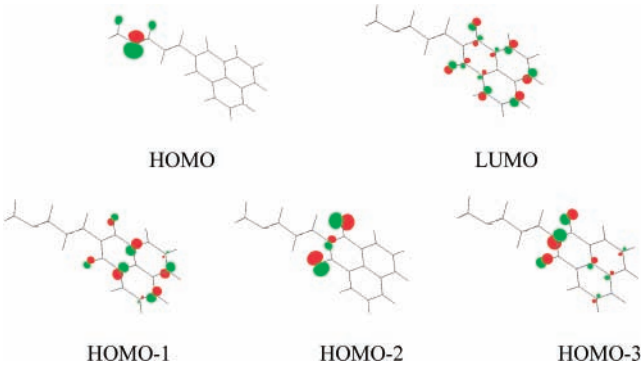

Figure 1. Frontier orbitals involved in the low-lying transitions of MNP.

that is attached to a self-assembling polypeptide.[31,50] It is seen from Figure 1 that the HOMO is an n-type orbital located mainly on the nitrogen atom, and the LUMO is a π^*-type orbital spreading on the naphthalimide chromophore. Hence the S_1 state is an n → π^* feature dominated by the HOMO → LUMO transition. Therefore, S_1 is formed due to the ET from the nitrogen atom to the naphthalimide moiety. The formation of S_1 more likely creates the radical pair, namely, the S_1 is a radical pair (RP) state. In acetonitrile, the transition energy of S_1 is 2.78 eV with the B3LYP functional and 3.02 eV with the MPW1PW91 functional. The S_2 state with a larger oscillator strength arises from the HOMO−1 → LUMO (π → π^*) transition, and its transition energy, 3.62 and 3.71 eV with B3LYP and MPW1PW91 functional, respectively, is slight higher than the experimental observation (3.51 eV). The orbital energy analysis shows that the orbital of HOMO−2 and HOMO−3 are nearly degenerated; therefore, these two molecular orbitals may change their order when the environment varies, e.g., in the polar solvent. This gives a reasonable explanation for the phenomena that the transition energy of HOMO−2 → LUMO is larger than that of HOMO−3 → LUMO in acetonitrile. The transition energy of T_1 is lower than that of the S_1 state both in the gas phase and in acetonitrile. Comparing with the gas-phase case, the transition energies in

TABLE 2: Geometry Parameters of MNP in the Ground and Excited States

state	$R(C_{10}-N_2)^a$	$A(C_{15}-N_2-C_{16})^b$	$A(C_{15}-N_2-H)$	$A(C_{15}-N_2-H)$	$D(C_{14}-C_{15}-N_2-C_{16})^c$	θ^d
ground	7.50	115.74	112.28	112.80	176.20°	
CT	7.48	123.15	118.36	118.01	154.56°	81.14°

[a] Center-to-center distance, in Å. [b] Bond angles in degrees. [c] Dihedral angles in degrees. [d] The orientation angle between the donor and the acceptor moieties.

TABLE 3: Emission Properties of MNP in the Gas Phase and in Acetonitrile[a]

	gas phase				acetonitrile					$\Delta G_{et}{}^b$	
state	dominant transition	E	f	μ	dominant transition	E	f	μ	$E_{exp}{}^c$	this work	exp[c]
T_1	HOMO → LUMO	2.00	/	4.11	HOMO → LUMO	2.01	/	6.29	2.29		
		1.96		4.09		1.98		6.25			
S_1	HOMO → LUMO	2.01	0.0001	31.72	HOMO → LUMO	2.06	0.0003	29.60	2.75	−0.99	−0.86
		2.27	0.0001	31.68		2.30	0.0002	29.57		−0.89	

[a] See the footnotes of Table 1 for the definitions of the symbols. [b] Free energy change (in eV) for the back ET. [c] Experimental data from the phosphorescence and fluorescence measurements, ref 31.

acetonitrile exhibit blue shifts. Maybe this phenomenon can be explained by the solvation energies. The nonequilibrium solvation energies in acetonitrile are smaller than that of the equilibrium ground state; hence the transition energies in acetonitrile present the blue shifts.

To inspect the properties of the excited states and the emission spectra, the geometries of the excited states should be optimized at first. However, the gradient optimization associated with TD-DFT is not available yet in the Gaussian program. Therefore, we turned to invoke the ab initio methods. Taking into account the computation cost and the feasibility in convergence, the configuration interaction singlet (CIS) method is suitable for the present purpose. Besides, by assuming the same equilibrium geometry for the CT states, S_1 and T_2, we performed the geometry optimization of the CT states. The excited-state geometry was obtained in acetonitrile with CIS method. The main parameters of center-to-center distance, bond angles, and dihedral angles of MNP for the ground and excited states were given in Table 2. When the optimized geometric parameters are compared with the ground-state structures, the bond angles and dihedral angles are distinct. For the optimized structure of excited CT state, the donor moiety is almost planar, and the orientation angle between the donor and the acceptor is found 81.14°. On the other hand, the donor moiety, SP1 (see Scheme 1 for the abbreviation), is pyramidal in the ground state. However, the comparison of these two optimal geometies exhibits a negligible change of the center-to-center distance.

On the basis of the optimal geometries, transition energies for emission processes from S_1 to S_0 in the gas phase and in acetonitrile were calculated at the levels of B3LYP/6-31G* and MPW1PW91/6-31G*. The transition energies, oscillator strengths, and dipole moments were listed in Table 3. Besides the CT state, the optimal geometry of T_1 state, which is a LE state, was optimized at the level of UB3LYP/6-31G* level. It is easy to see that the transition energy is lower than that of S_1 state both in the gas phase and in acetonitrile, which is accordant with the experimental observation. In acetonitrile, the transition energy of the T_1 state is 2.01 eV with the B3LYP functional and 1.98 eV with the MPW1PW91 functional, being lower than the transition energy of the naphthalimide triplet state (2.29 eV) observed experimentally.[31] With the inspection of the dipole moment, S_1 is clearly a CT state, and the calculated transition energies are lower than the experimental measurements by around 0.50 eV. Polarity of the solvents affects the transition energies, and the transition energies in acetonitrile exhibit blue shifts comparing with the gas-phase case. In acetonitrile, the electrostatic solvation energies of ground state are calculated to be −13.65 kcal/mol with the B3LYP functional and −14.45 kcal/mol with the MPW1PW91 functional, but for the excited state the values are −8.74 and −9.79 kcal/mol, respectively. This is somewhat unusual; maybe the reason is based on the given system or the method itself.

In the aspect of experiment, the free energy change ΔG_{et} associated with the ET electron transfer can be evaluated using the Rehm−Weller equation[51]

$$\Delta G_{et} = e(E^0_{ox} - E^0_{red}) - E_{00} - \frac{e^2}{\epsilon_s r} \qquad (6)$$

where E^0_{ox} and E^0_{red} are oxidation and reduction potentials for the donor and acceptor, respectively, and E_{00} denotes the excitation energy. The last term in eq 6 is the work required to bring the donor and acceptor to the ET distance, with e being the unit charge, r the distance between the acceptor and donor, and ϵ_s the static dielectric constant of the polar solvent. The driving force for the photoinduced electron transfer of MNP using eq 6 was experimentally estimated.[31] The reduction potential of 1,8-naphthalimide is reported −1.44V vs SCE in acetonitrile, and the secondary amine in the spermine chain is reported to be 1.31 V vs SCE. Adding the Columbic term of 0.10 eV, ΔG_{et} is estimated to be −0.86 eV. Unlike the experimental measurement, the determination of this quantity is straightforward in our calculation. The free energy change of the S_1 state is −0.99 eV with the B3LYP functional and −0.89 eV with the MPW1PW91 functional, agreeing well with experimental data.

A profile of the energy levels for the singlet excited states, the triplet states, and the CT state is essential for the understanding of the ET process of MNP. Such a profile for the low-lying CT radical pair (RP) states in acetonitrile was shown in Figure 2. The energy level of the RP state lies higher than the T_1 state. Actually, the absorption of naphthalimide triplet and radical anion transients in acetonitrile can be observed through the photolysis experiment. From Figure 2 it is easy to find that the free energy changes of the charge recombination ΔG_{CR} in acetonitrile are −2.62 and −2.82 eV with the B3LYP and MPW1PW91 functionals, respectively.

Judging from the oscillator strengths and inspecting the state energy levels of the excited states, we may draw a conclusion that the direct photoexcitation more likely drives MNP from the ground state to S_2 in acetonitrile, owing to the apparently dominant oscillator strengths. Our calculation unambiguously revealed the initial state of the ET process. Combining the experimental observations and the values of ΔG_{et} (see Table

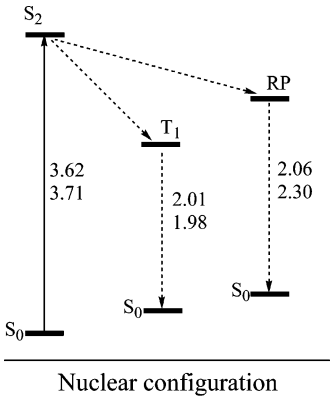

Figure 2. . Schematic energy diagram for the decay from S_2 of MNP in acetonitrile: (top) by TD-B3LYP/6-31G*; (bottom) by TD-MPW1PW91/6-31G*. The transition energy is given in electronvolts.

3), we can summarize the processes of ET and the charge recombination (CR) as Figure 2.

Photoexcitation of BNS. There are a number of conformations for the BNS system, but two among them are representative, the linear structure and the stacked one. The stacked conformation allows the maximum overlap between π-type molecular orbitals in two naphthalimide chromophores, and hence it is more stable than any linear conformations. According to Jones et al., the proximity of two naphthalimide rings in BNS should play an important role in the generation of the radical anion.[31] Baptista and co-workers suggested that a silica-gel conjugate of *N*,*N*′-bis(2-phosphonoethyl)-1,4,5,8-naphthalenediimide will generate a radical anion by enforcing two diimide chromophores close to each other.[52] In this work, the stacked conformation of BNS was optimized at the B3LYP/6-31G level. In BNS, the electron transition is much more complicated than a single naphthalimide chromophore, so we calculated 11 singlet states for BNS in the gas phase and in acetonitrile. The transition energies, the oscillator strengths, and the dipole moments in different directions were listed in Table 4. The frontier orbitals involved in the low-lying transitions of BNS were illustrated in Figure 3 as well.

Most interestingly, the low-lying excited states of the BNS can be classified into three types. The states S_1, S_2, S_3, and S_4 belong to CT states that result from the ET between the dialkylamine moiety and the naphthalimide chromophore. In these four states the dialkylamine moiety acts as an electron donor and the naphthalimide chromophore as an acceptor. The S_5 and S_{11} states are also CT states, but the ET takes place between the two terminal naphthalimide chromophores. The ET reactions in these two states are in the opposite direction. The other states are due to the local excitation. The corresponding characters of CT states of BNS in the gas phase were summarized in Figure 4.

As mentioned above, the S_1 state is responsible for the transition from the HOMO to the LUMO, and the HOMO is an n-type orbital mainly located on the nitrogen atom in the bridge. On the other hand, the LUMO and LUMO+1 are π*-type orbitals localized on the right-hand side (abbreviated as NP2; see Scheme 1) and left-hand side (NP1) naphthalimide chromophores, respectively. The next three states are similar to the S_1 state and their transition characters were listed in Table 4. The large values of the total dipole moments indicate the ET character. Furthermore, S_5 and S_{11} states exhibit the ET character with an even longer distance. The forward and backward ET reactions between the two naphthalimide chromophores happen in these two cases. This is interesting if we note the ET feature summarized in Figure 4. The S_5 state arises from the transition from HOMO−2 to LUMO and S_{11} is from HOMO−3 to LUMO+1. From Figure 3, one can note that all the orbitals concerned, LUMO+1, LUMO, HOMO−2, and HOMO−3, are π-type, but HOMO−2 and LUMO+1 locate on the NP1 and LUMO and HOMO−3 locate on NP2. The features of the two states, S_5 and S_{11}, are similar. Seen from the *x*, *y*, and *z* component of the dipole moments, the S_5 state results from an ET from NP2 to NP1, and the S_{11} state has the reverse manner. As shown in Figure 3 and Table 4, the S_6 state is a LE state resulted from the transition from HOMO−4 to LUMO+1, due to the n $\rightarrow \pi^*$ transition. This state corresponds to the S_2 state of the monomer MNP. The transition energy of this state matches the value of S_2 state of MNP, 3.50 eV (see Table 1). S_{10} exhibits the largest oscillator strength among all the concerned states. The molecular orbital analysis shows that it is the LE state corresponding to the S_3 of MNP.

Because the absorption spectra of BNS were detected experimentally in acetonitrile,[31] we made a more detailed discussion on the electronic structure of the low-lying states in solution here. Transition energies of the low-lying excited states of BNS in acetonitrile were computed by TD-DFT associated with PCM. The frontier orbitals involved in the low-lying transition of BNS in acetonitrile were depicted in Figure 5, but only those differing from the gas phase were given. Seen from Figure 3 and Figure 5, HOMO and HOMO−1 of the frontier orbitals of BNS are different in the gas phase and in acetonitrile. In the gas phase, the HOMO is an n-type orbital located mainly on one of the nitrogen atoms of the dialkylamine moiety. In acetonitrile, the HOMO is also an n-type orbital, but it delocalizes on the two nitrogen atoms of the dialkylamine moiety. It is the same case as HOMO−1.

The vertical excitation energies, the oscillator strengths, and transition dipole moments of the low-lying 11 singlet states were reported in Table 4. For the sake of comparison, the energy and dipole moment of the triplet state T_1 were also calculated. It is noticeable that the states S_1, S_2, S_3, and S_4 are the CT states and the charge separation occurs between the naphthalimide group and bridge group of dialkylamine. Because of the negligible oscillator strengths and the relatively lower excited energies for these four states, it seems that the corresponding absorption bands are hardly observed in experiment. The S_1 state results from the transition from HOMO to LUMO, and the ET is from the bridge to the NP2 moiety. The S_3 state is formed a the similar way, but with a larger dipole moment, 37.53 D. The S_2 state arises from the transition from HOMO to LUMO+1, and the ET is from the bridge to the NP1 moiety. The transition character of S_4 is similar to that of S_2. The orbital energy analysis showed that the energies of LUMO and LUMO+1 are nearly degenerated, so the transition energy of S_3 is close to S_4.

A remarkable feature worthy of noticing is the CT state, in which electron transfer from NP2 to NP1 falls from S_{11} in the gas phase to S_6 in acetonitrile. The S_5 state with a large dipole moment arises from the transition from HOMO−2 to LUMO, and hence it is also a CT state. The transition feature of S_6 is similar to that of S_5, but the ET proceeds in the opposite direction. From intuition, S_5 and S_6 should be degenerated in energy. A difference of 0.16 eV eliminates the degeneracy of these two states. The corresponding dipole moments for both S_5 and S_6 in acetonitrile are larger than those in the gas phase because of the mutual polarizations between the solute and the environment. The S_6 state has the largest oscillator strength (0.0110) among all the CT states in acetonitrile. In experiment, the absorption band of the naphthalimide radical anion at 410

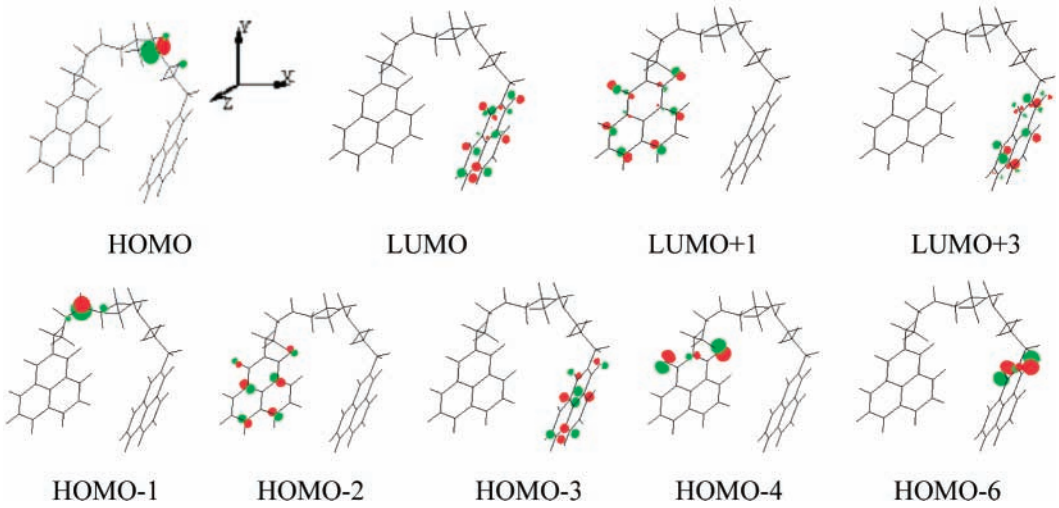

Figure 3. Schematic drawings of frontier orbitals involved in the low-lying states of stacked BNS.

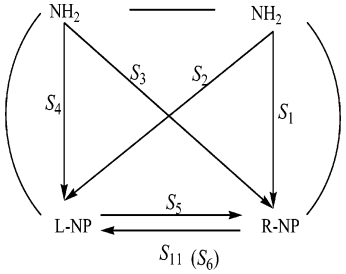

Figure 4. Depiction of the itineraries of ET among the low-lying states. See Scheme 1 for the notations of the chromophore groups. The arrow indicates the direction of the ET for the specified excited state when the system undergoes a transition from the ground state to the specified state. S_6 in the parenthesis indicates the state assigned in acetonitrile.

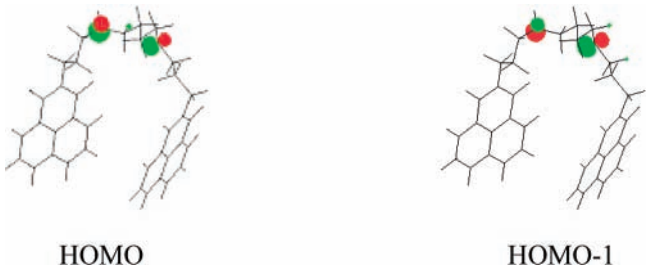

Figure 5. Schematic drawings of frontier orbitals involved in the low-lying transitions of BNS in acetonitrile. The drawings of LUMO, LUMO+1, HOMO−2, and HOMO−3 are similar to those in the gas phase and are omitted here.

nm was observed, and this indicates that intramolecular ET of BNS system can create a naphthalimide radical pair.[31,53] However, the radical cation of 1,8-naphthalimide was not detected in experiment. It might be attributed to the very weak absorption of the cation. Through photoexcitation of BNS, it is possible to produce the naphthalimide radical anion via the formation of CT state. On the basis of this investigation, S_6 is more likely formed in the excitation process, because it has the largest oscillator strength among all the CT states. Also, this yields a reasonable explanation for the mechanism of the intramolecular ET of BNS system. Through analysis it becomes clear that the CT state is formed via intra-naphthalimide-pair ET; that is, the naphthalimide radical anion is formed during this process but does not arise from an ET between the dialkylamine moiety and the naphthalimide moiety.

The comparison of the theoretical calculation with the experimental spectrum shows that S_8 is responsible for the 340

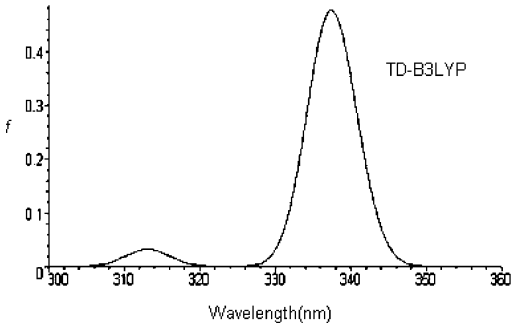

Figure 6. Absorption spectra of BNS system using TD-B3LYP/6-31G in acetonitrile. The oscillator strength is given as the height of the peak.

nm absorption of the $\pi \rightarrow \pi^*$ transition. Moreover, the results from the calculation in the gas phase show that the S_{10} is the most intense absorption. In the presence of polar solvents, this state turns out to be S_8. These results coincide with the experimental observations. From the calculated results, we found there are other $\pi \rightarrow \pi^*$ transitions (see Table 4, Figure 3, and Figure 5), but their oscillator strengths are very small or their energies are degenerated; hence they are invisible. For example, S_7 arises from a $\pi \rightarrow \pi^*$ transition and the transition energy is almost degenerated with that of S_8, and therefore these two states cannot be distinguished. From the theoretical calculation, the simulated absorption spectra with different functions can be obtained by broadening the theoretical line spectra with Gaussian function, i.e.,

$$I(\lambda) \approx \sum_i f_i \exp\left[-\frac{1}{2}\left(\frac{\tilde{\lambda} - \tilde{\lambda}_i}{\sigma}\right)^2\right] \qquad (7)$$

where σ is the width of the Gaussions centered at peak number i with wavelength $\tilde{\lambda}_i$ and oscillator strength f_i. According to eq 7, the simulation was given in Figure 6. The strongest band is the 340 nm absorption of naphthalimide chromophore. As for Figure 6, we assigned the intense low-energy peak at 337 nm to the HOMO−2 → LUMO+1 transition. It seems that this peak corresponds to the experimentally observed maximum absorption at 340 nm from the LE of the naphthalimide chromophore. However, the B3LYP functionals predict a small peak at about 313 nm that was not reported in the experiment. A possible reason is the too weak oscillator strength.

Comparing the relative energies of the excited states in the gas phase and in solution (see Table 4), we find that the solvent

TABLE 4: Energies of the Low-Lying Excited States of BNS in the Gas Phase and in Acetonitrile[a]

state	transition	E[b]	f[c]	m_{0i}[d]	μ_x	μ_y	μ_z	μ_{tot}[e]	H_{0i}[f]
T_1	HOMO → LUMO	2.54	/	/	−0.60	−2.93	1.78	3.48	/
	HOMO → LUMO	2.53	/	/	−0.33	−7.86	3.58	8.64	/
S_1	HOMO → LUMO	2.01	0.0002	0.07	−9.65	20.80	−8.26	24.38	0.008
	HOMO → LUMO	2.36	0.0003	0.19	−9.99	17.10	−6.95	20.98	0.031
S_2	HOMO → LUMO+1	2.28	$<10^{-4}$	0.01	22.80	24.67	−1.84	33.64	0.001
	HOMO → LUMO+1	2.44	0.0004	0.20	0.83	21.35	9.87	23.53	0.030
S_3	HOMO−1 → LUMO	2.42	$<10^{-4}$	0.01	−32.87	21.70	2.91	39.50	0.001
	HOMO−1 → LUMO	2.50	$<10^{-4}$	0.03	−32.7	17.99	3.93	37.53	0.002
S_4	HOMO−1 → LUMO+1	2.48	0.0003	0.07	0.01	25.01	9.27	26.67	0.009
	HOMO−1 → LUMO+1	2.53	0.0001	0.08	22.30	21.01	−0.64	30.64	0.008
S_5	HOMO−2 → LUMO	3.42	0.0001	0.04	−30.72	−11.10	−3.98	32.90	0.005
	HOMO−2 → LUMO	3.47	0.0008	0.25	−30.65	−14.97	−2.81	34.23	0.032
S_6	HOMO−4 → LUMO+1	3.49	0.0002	0.05	−1.16	3.72	3.22	5.05	0.101
	HOMO−3 → LUMO+1	3.63	0.0110	0.89	30.13	−7.84	10.57	32.88	0.124
S_7	HOMO−6 → LUMO	3.50	0.0002	0.05	2.98	2.22	−2.37	4.41	0.074
	HOMO−3 → LUMO	3.65	0.1186	2.93	2.49	−11.00	5.25	12.44	1.313
S_8	HOMO−3 → LUMO	3.75	0.0415	0.67	−2.60	1.70	−0.03	3.10	0.642
	HOMO−2 → LUMO+1	3.68	0.3833	5.24	2.63	−10.97	3.96	11.96	1.650
S_9	HOMO → LUMO+3	3.76	0.0207	0.47	−6.12	10.10	−3.47	12.31	0.315
	HOMO−6 → LUMO+1	3.71	0.0093	0.32	0.06	0.12	3.76	3.76	0.385
S_{10}	HOMO−2 → LUMO+1	3.79	0.2981	1.79	4.68	−7.00	3.93	9.29	1.552
	HOMO−8 → LUMO+1	3.78	0.0004	0.07	2.90	−1.49	−1.24	3.49	0.080
S_{11}	HOMO−3 → LUMO+1	3.81	0.0356	0.62	28.83	−4.10	9.38	30.59	0.099
	HOMO−5 → LUMO	3.96	0.0327	0.58	0.36	−10.24	4.42	11.15	0.508

[a] See the footnotes of Table 1 for the definition of symbols. The first line is for the gas phase and the second line is the result in acetonitrile. The calculations are performed at the level of B3LYP/6-31G. [b] Relative energy (in eV) of ground state S_0 is taken as zero. The energy of ground state is −1835.60091 au in the gas phase and −1835.63770 au in acetonitrile. [c] Oscillator strengths. [d] Transition dipole form the ground state to the specified state. [e] The dipole moments of ground state are 6.28 and 6.78 Debyes in the gas phase and acetonitrile, respectively. The direction of the dipole is shown in Figure 3. [f] Electronic coupling matrix element between the ground state and the specified one (in eV).

effect produces blue shifts on absorption spectra with respect to the gas-phase ones but has little influence on the oscillator strength and transition dipole moment. In acetonitrile, the energy order and transition features of the lowest five CT states repeat those in the gas phase, but the discrepancy emerges in the next states. The LE state S_8 of gas phase becomes S_7 and S_{10} changes to S_8 in acetonitrile, and the CT state S_{11} in the gas phase finds its position at S_6 in acetonitrile. In acetonitrile the two LE states S_7 and S_8 are degenerated in energy and it is difficult to distinguish one from the other. Both states have the $\pi \rightarrow \pi^*$ transition feature. In the S_7 state, the electron delocalizes in the NP2 chromophore; in a similar way, the delocalization occurs in the chromophore NP1 in S_8. In experiment, an absorption band at 340 nm was observed in acetonitrile,[54] and it is more likely the S_8 state in our calcualtion. This state has the largest oscillator strength and the $\pi \rightarrow \pi^*$ character. The calculated transition energy fits well with the experimental one.[31] The transition type of S_8 for BNS in acetonitrile is similar to that of S_2 of MNP. This band was identified as the LE state in both MNP and BNS ($\lambda = 340$ nm[31]). The present calculation reveals the information that the CT bands with longer wavelengths have been missed in the measurements. For a system NP−$(CH_2)_3$-$NH(CH_2)_4NH(CH_2)_3NH_2$, which is formed by replacing one NP group with $-NH_2$ in BNS (see Scheme 1), only the absorption from the excited triplet state was observed in all cases, indicating no evidence of a naphthalimide radical anion owing to dimer excitation. No absorption is found for this system in the range of $\lambda > 400$ nm (<3.10 eV).[55] This means that the transition bands of CT between NP and spermine are unable to be detected. Seen from the oscillator strengths as given in Table 4, the absorbencies of CT transitions are too weak to be observed. This gives a satisfied explanation of the experimental phenomena. Besides, the energy level of the T_1 state in acetonitrile is close to the one in the gas phase.

Furthermore, we paid attention to the ET dynamics through the electronic coupling matrix element H_{ij}. The values of H_{ij} for the transition between the ground state and the excited states were calculated using eq 5 and were listed in Table 4. It is obvious that the values of H_{07} and H_{08} are much larger than those of others in acetonitrile. According to Fermi's golden rule, the ET rate constant is proportional to the square of H_{ij}. Hence the ET rate from the ground state to S_7 and S_8 states can be predicted much faster than those of others. On the basis of theoretical calculations, we knew both S_7 and S_8 are LE states; therefore, it seems that the ET rate from the ground state to the LE state is much faster than that to CT states. Thus, these results enable us to make a prediction that the LE state is produced first and its population will be much larger than that of the CT state in the primary photoexcitation process. This implies that the absorption maximum is due to LE rather than CT excitation. The above discussions also confirm that the detected absorption spectrum at 340 nm is due to an LE transition located on the naphthalimide chromophores.

Conclusions

In this work, the geometries of BNS and MNP systems were optimized and the stacked conformation of BNS was investigated using DFT, to gain insight into the mechanism of the photoinduced ET and the electronic structures of excited states. The excited electronic states of MNP were studied and its absorption properties were compared with those of BNS. From the calculations, we made clear the energy levels of the excited states and then proposed the excitation mechanisms. In the title system, there are four sites where an electron can be removed or be trapped. It is just the multichannels of ET that make the excitations of the molecule and the decay of the excited states complicated.

The calculations performed for the MNP system suggest that the ET of excited state is initiated from S_3 in the gas phase and S_2 in acetonitrile, owing to the apparently dominant oscillator strengths. However, the molecular orbital analysis shows both

S_3 in the gas phase and S_2 in acetonitrile result from the transition of HOMO−1 to LUMO. From this locally excited state, the ET from the dialkylamine moiety to the naphthalimide chromophore follows. Thus the system decays to the lowest singlet state or triplet state, where the system is quenched to the ground state though the emission of fluorescence or phosphorescence. A comparative discussion with the experimental data confirms our postulations.

The theoretical results agree well with the experimental data. In the absorption spectrum of MNP, T_2 and S_1 are both CT states. In acetonitrile the S_2 state is assigned to the absorption at 340 nm, and the calculated result is very close to the experimental data. In the case of the emission spectrum calculation, the transition energies of the singlet and triplet states both agree well with the experimental value. In addition, the driving force for photoinduced ET in MNP indicates that it is sufficient for ET process to occur.

Through this study, the mechanism of the intramolecular ET of the BNS system becomes clear. There exist three types of excited states in BNS. The first type is characterized by the electron transferring between the naphthalimide chromophore moiety and the dialkylamine, the second type is characterized by the electron transferring between the two terminal naphthalimide chromophore moieties, and the last type is featured by the electronic excitation delocalized within either the left chromophore or the right one. The first two types are CT states and the third one belongs to LE. Through the analysis of molecular orbitals and the features of excited states, it seems that the naphthalimide radical anion is formed via intra-naphthalimide-pair ET but does not arise from an ET between the dialkylamine moiety and the naphthalimide moiety. The latter was one of the proposals introduced in literature.[31] In addition, based on the study of the transition feature and the electronic coupling matrix element calculations using GMH theory, it is clear that the main absorption of the BNS system is attributed to the LE absorption with $\pi \rightarrow \pi^*$ character.

Acknowledgment. This work is supported by National Natural Science Foundation of China (Nos. 20572073, 20533070).

References and Notes

(1) Chen, K. Y.; Hsieh, C. C.; Cheng, Y. M.; Lai, C. H.; Chou, P. T.; Chow, T. J. *J. Phys. Chem. A* **2006**, *110*, 12136.
(2) Chow, T. J.; Pan, Y. T.; Yeh, Y. S.; Wen, Y. S.; Chen, K. Y.; Chou, P. T. *Tetrahedron* **2005**, *61*, 6967.
(3) Yamaguchi, S.; Yoshimura, I.; Kohira, T.; Tamaru, S. I.; Hamachi, I. *J. Am. Chem. Soc.* **2005**, *127*, 11835.
(4) Terazono, Y.; Kodis, G.; Andreasson, J.; Jeong, G.; Brune, A.; Hartmann, T.; Du1rr, H.; Moore, A. L.; Moore, T. A.; Gust, D. *J. Phys. Chem. B* **2004**, *108*, 1812.
(5) Sumida, J. P.; Liddell, P. A.; Lin, S.; Macpherson, A. N.; Seely, G. R.; Moore, A. L.; Moore, T. A.; Gust, D. *J. Phys. Chem. A* **1998**, *102*, 5512.
(6) Bailly, C.; Carrasco, C.; Joubert, A.; Bal, C.; Wattez, N.; Hildebrand, M. P.; Lansiaux, A.; Closon, P.; Houssier, C.; Cacho, M.; Ramos, A.; Brana, M. F. *Biochemistry* **2003**, *42*, 4136.
(7) Kaur, J.; Ghosh, N. N.; Chandra, R. *Chem. Pharm. Bull*. **2004**, *52*, 316.
(8) Chen, S. F.; Behrens, D. L.; Behrens, C. H.; Czerniak, P. M.; Dexter, D. L.; Dusak, B. L. *Anti-Cancer Drugs* **1993**, *4*, 447.
(9) Ghosh, S. K.; Hossain, S. U.; Bhattacharya, S.; Bhattacharya, S. C. *J. Photochem. Photobiol. B* **2005**, *81*, 121.
(10) Lai, C. M.; Garner, D. M.; Gray, J. E.; Brogdon, B. L.; Peterman, V. C.; Pieniaszek, H. J., Jr. *J. Pharm. Biomed. Anal*. **1998**, *17*, 427.
(11) Saito, I.; Takayama, M.; Sugiyama, H.; Nakatani, K.; Tsuchida, A.; Yamamoto, M. *J. Am. Chem. Soc.* **1995**, *117*, 6406.
(12) Rogers, J. E.; Kelly, L. A. *J. Am. Chem. Soc.* **1999**, *121*, 3854.
(13) Rogers, J. E.; Weiss, S. J.; Kelly, L. A. *J. Am. Chem. Soc.* **2000**, *122*, 427.
(14) Aveline, B. M.; Matsugo, S.; Redmond, R. W. *J. Am. Chem. Soc.* **1997**, *119*, 11785.
(15) Kawai, K.; Osakada, Y.; Fujitsuka, M.; Majima, T. *J. Phys. Chem. B* **2007**, *111*, 2322.
(16) Saito, I.; Takayama, M.; Kawanishi, S. *J. Am. Chem. Soc.* **1995**, *117*, 5590.
(17) Steward, W. W. *Nature* **1981**, *292*, 17.
(18) Marling, J. B.; Hawley, J. G.; Liston, E. M.; Grant, B. *Appl. Opt.* **1974**, *13*, 2317.
(19) Middleton, R. W.; Parrick, J. *J. Heterocycl. Chem.* **1985**, *22*, 1567.
(20) Middleton, R. W.; Parrick, J. *J. Heterocycl. Chem.* **1986**, *23*, 849.
(21) Daffy, L. M.; Silva, A. P.; de Gunaratne, H. Q. N.; Huber, C.; Lynch, P. L. M.; Werner; T.; Wolfbeis, O. S. *Chem. Eur. J.* **1998**, *4*, 1810.
(22) Ramachandram, B.; Saroja, G.; Sankaran, N. B.; Samanta, A. *J. Phys. Chem. B* **2000**, *104*, 11824.
(23) Gunnlaugsson, T.; Lee, C. T.; Parkesh, R. *Org. Biomol. Chem.* **2003**, *1*, 3265.
(24) Licchelli, M.; Biroli, A. O.; Poggi, A.; Sacchi, D.; Sangermani, C.; Zema, M. *J. Chem. Soc. Dalton Trans.* **2003**, 4537.
(25) Abad, S.; Kluciar, M.; Miranda, M. A.; Pischel, U. *J. Org. Chem.* **2005**, *70*, 10565.
(26) Poteau, X.; Brown, A. I.; Brown, R. G.; naHolmes, C.; Matthew, D. *Dyes Pigments* **2000**, *47*, 91.
(27) Aveline, B. M.; Matsugo, S.; Redmond, R. W. *J. Am. Chem. Soc.* **1997**, *119*, 11785.
(28) Brana, M. F.; Castellano, J. M.; Moran, M. *Anti-Cancer Drug Des.* **1993**, *8*, 257.
(29) Brana, M. F.; Castellano, J. M.; Moran, M.; Perez de Vega, M. J.; Qian, X. D.; Romerdahl, C. R.; Keihauer, G. *Eur. J. Med. Chem*. **1995**, *30*, 235.
(30) Lin, P. K. T.; Pavlov, V. A. *Bioorg. Med. Chem. Lett.* **2000**, *10*, 1609.
(31) Jones, G., II; Kumar, S. *J. Photochem. Photobiol. A* **2003**, *160*, 139.
(32) Newton, M. D. *Chem. Rev*. **1991**, *91*, 767.
(33) Mikkelsen, K. V.; Ratner, M. A. *Chem. Rev.* **1987**, *87*, 113.
(34) Kestner, N. R.; Logan, J.; Jortner, J. *J. Phys. Chem*. **1974**, *78*, 2148.
(35) Efrima, S.; Bixon, M. *Chem. Phys*. **1976**, *13*, 447.
(36) Jortner, J. *J. Chem. Phys.* **1976**, *64*, 4860.
(37) Cave, R. J.; Newton, M. D. *Chem. Phys. Lett.* **1996**, *249*, 15.
(38) Adamo, C.; Barone, V. *Chem. Phys. Lett.* **2000**, *330*, 152.
(39) Jödicke, C. J.; Lüthi, H. P. *J. Chem. Phys.* **2002**, *117*, 4146.
(40) Scholz, R.; Kobitski, A. Y.; Zahn, D. R. T.; Schreiber, M. *Phys. Rev. B* **2005**, *72*, 245208.
(41) Neiss, C.; Saalfrank, P.; Parac, M.; Grimme, S. *J. Phys. Chem. A* **2003**, *107*, 140.
(42) Li, X. Y.; Fu, K. X. *J. Theor. Comput. Chem.* **2005**, *4*, 907.
(43) Li, X. Y.; Fu, K. X.; Zhu, Q.; Shan, M. H. *J. Comput. Chem.* **2004**, *25*, 835.
(44) Fu, K. X.; Zhu, Q.; Li, X. Y.; Gong, Z.; Ma, J. Y.; He, R. X. *J. Comput. Chem.* **2006**, *27*, 368.
(45) Miertus, S.; Scrocco, E.; Tomasi, J. *Chem. Phys.* **1981**, *55*, 117.
(46) Cossi, M.; Barone, V.; Mennucci, B.; Tomasi, J. *Chem. Phys. Lett*. **1998**, *286*, 253.
(47) Barone, V.; Cossi, M. *J. Phys. Chem. A* **1998**, *102*, 1995.
(48) Frisch, M. J.; Trucks, G. W.; Schlegel, H. B.; et al. *Gaussian 03*, revision B.03; Gaussian Inc.: Pittsburgh, PA, 2003.
(49) Kohn, W. *Phys. Rev. Lett.* **1996**, *76*, 3168.
(50) Jones, G., II; Vullev, V. I. *J. Phys. Chem. A* **2001**, *105*, 6402.
(51) Rhem, D.; Weller, A. *Isr. J. Chem.* **1970**, 259.
(52) Demeter, A.; Biczók, L.; Bérces, T.; Wintgens, V. *J. Phys. Chem.* **1993**, *97*, 3217.
(53) Rodrigues, M. A.; Tada, D. B.; Politi, M. J.; Brochsztain, S.; Baptista, M. S. *J. Non-Cryst. Solids.* **2002**, *304*, 116.
(54) Pena, V. A.; de la Pardo, A.; Poyato, J. M. L. *Int. J. Quantum. Chem.* **2003**, *91*, 446.
(55) McMasters, S.; Kelly, L. A. *J. Phys. Chem. B* **2006**, *110*, 1046.